3 Generalized Newtonian Fluid (GNF) Models

As discussed in Chapter 2, most polymers exhibit *shear thinning*, temperature and pressure dependent viscosities. The shear thinning effect is defined as the reduction in viscosity at high rates of deformation. This phenomenon is explained by the fact that the molecular chains are disentangled and stretched out at high rates of deformation and can therefore slide past each other with more ease, which in turn lowers the bulk viscosity of the melt. Figure 3.1 clearly shows the shear thinning behavior and temperature dependence of the viscosity of a general purpose polystyrene.

To take these *non-Newtonian effects* into consideration while neglecting the viscoelastic effects[1], it is common to define the viscosity η as a function of the strain rate and temperature. To calculate the deviatoric stress tensor in the momentum balance (see Chapter 4), we can then write

$$\underline{\underline{\tau}} = \eta\left(\dot{\gamma}, T\right)\underline{\underline{\dot{\gamma}}} \tag{3.1}$$

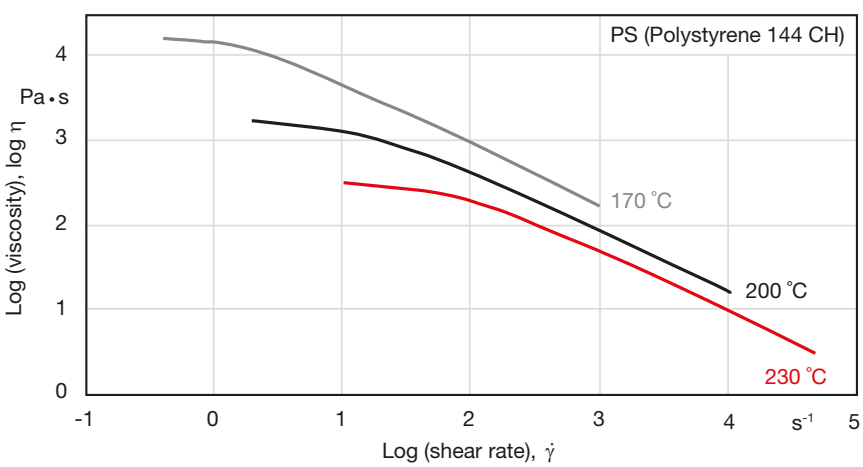

Figure 3.1 Viscosity curves for a polystyrene

[1] The Deborah number, Eq. 1.16, defined as the product $De = \lambda\omega$, reflects the degree of viscoelasticity. Newtonian behavior is characterized by low *De* values.

This equation is often referred to as the *Generalized Newtonian Fluid* model. Here, $\underline{\underline{\dot{\gamma}}}$ is the *strain rate* or *rate of deformation tensor* defined by

$$\underline{\underline{\dot{\gamma}}} = \nabla \underline{u} + \nabla \underline{u}^t \tag{3.2}$$

where $\nabla \underline{u}$ represents the velocity gradient tensor, defined in Chapter 1.

Constitutive equations based on generalized Newtonian fluid models differ in their shear thinning expression, but they all require that the non-Newtonian viscosity $\eta(\dot{\gamma})$ is a function of the three scalar invariants of the strain rate tensor. Because of the incompressibility of polymer melts, the first invariant, defined by the sum of the diagonal terms of the tensor, equals zero (I = 0), and assuming steady shear flow, the third invariant, defined by the determinant of the tensor, also equals zero (III = 0). Therefore, $\eta(\dot{\gamma})$ is only a function of the second invariant, II. This is expressed by the magnitude of $\dot{\gamma}$ and can be written as

$$\dot{\gamma} = \sqrt{\frac{1}{2}\text{II}} \tag{3.3}$$

where $\dot{\gamma}$ is the magnitude of the strain rate tensor in Eq. 3.1. The second invariant of the strain rate tensor is defined as

$$\text{II} = \sum_i \sum_j \dot{\gamma}_{ij}\, \dot{\gamma}_{ji} \tag{3.4}$$

The strain rate tensor components in Eq. 3.4 are defined by

$$\dot{\gamma}_{ij} = \frac{\partial u_i}{\partial x_j} + \frac{\partial u_j}{\partial x_i} \tag{3.5}$$

Numerous models describe the shear thinning, temperature and pressure dependence of polymer viscosity. Most are similar and based on the same assumptions; however, the different nomenclatures used make it difficult to distinguish between them. To add to the confusion, different names or combination of names are used. In this chapter, the most common models are presented and the connections to other models are highlighted. The temperature dependence is typically modeled in two different ways and these two approaches are explained in a general form in the following section. Due to the recent need for high pressure injection molding of thin products, a relatively new research area in the field of rheology is the pressure dependence of the viscosity. This topic will be addressed separately after the introduction of the viscous flow models. The description of the modeling of filled (Section 3.4) as well as cross-linking polymers (Section 3.5) will be expanded separately at the end of the chapter with more general comments that pertain to these systems.

3.1 Temperature Dependence of Viscosity

In addition to the strain rate dependence, the temperature dependence of the viscosity is expressed as a function separate from the rate of deformation dependence. This can be written as

$$\eta(T,\dot{\gamma}) = f(T)\,\eta(\dot{\gamma}) \tag{3.6}$$

where for small variations in temperature, $f(T)$ is often approximated using an exponential function such as

$$f(T) = \exp\left[-a\,(T - T_0)\right] \tag{3.7}$$

In the above equation, a is the temperature sensitivity of the viscosity, T is the temperature at which the viscosity is sought, and T_0 is a reference temperature, at which the viscosity is known. However, as mentioned in Chapter 2, a variation in temperature corresponds to a shift in the time scale when determining characteristic relaxation times within the polymer melt. There are two additional models that can be used, depending on the specific material processed and the desired temperature range: the Arrhenius shift and the WLF shift. The Arrhenius shift [1], which applies to semi-crystalline polymers, is written as

$$a_T(T) = \frac{\eta_0(T)}{\eta_0(T_0)} = \exp\left[\frac{E_0}{R}\left(\frac{1}{T} - \frac{1}{T_0}\right)\right] \tag{3.8}$$

where E_0 is the activation energy, T_0 a reference temperature, and R the gas constant. Using this shift, the viscosity curves measured at different temperatures can be used to generate a master curve at a specific temperature. Figure 3.2 [2] shows the viscosity of a low density polyethylene, for which the measured values were shifted to a reference temperature of 150 °C. For the shift in Figure 3.2, an activation energy of E_0 = 54 kJ/mol was used.

For amorphous thermoplastics, the Arrhenius shift is valid for temperatures $T > T_g$ + 100 K. Below this temperature, free volume effects dominate the behavior. Hence, for lower temperatures, the temperature dependence of the viscosity of amorphous thermoplastics is best described by the Williams-Landel-Ferry (WLF) equation [3, 4]. This equation describes the viscosity η of the polymer at any given temperature, T, in relation to a reference viscosity at a reference temperature, T_s

$$\log a_T(T) = \log\frac{\eta_0(T)}{\eta_0(T_s)} = \frac{-C_1\,(T - T_s)}{C_2 + T - T_s} \tag{3.9}$$

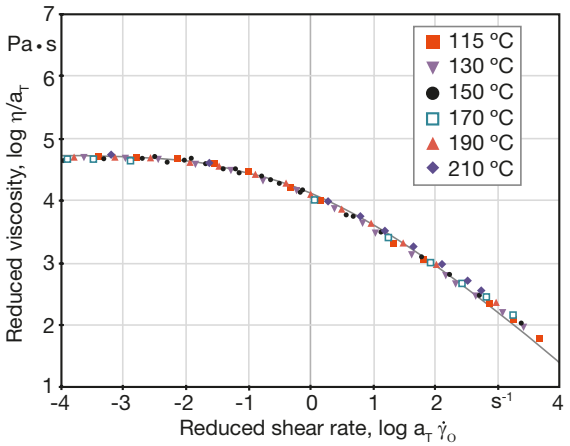

Figure 3.2 Reduced viscosity curve for a low density polyethylene (LDPE) at a reference temperature of 150 °C.

For polymers, this equation holds true only in the zero shear viscosity region. Because T_g is a widely used temperature, it is often chosen as the reference temperature T_s with $C_1 = 17.44$ and $C_2 = 51.6$ K. T_g is much lower than typical processing temperatures, therefore, van Krevelen [5] proposed a better alternative for T_s using $T_s = T_g + 43$ K, resulting in $C_1 = 8.86$ and $C_2 = 101.6$ K. Usually, the viscosity is not known at the reference temperature T_s, but at a temperature in the processing temperature range T^*, so that a second shift between measurement or processing temperature T^* and the reference temperature T_s is required. Equation 3.10 presents the relation between viscosity at T^* and at the actual temperature T

$$\log \frac{\eta_0(T)}{\eta_0(T^*)} = \frac{8.86\,(T^* - T_s)}{101.6 + T^* - T_s} - \frac{8.86\,(T - T_s)}{101.6 + T - T_s} \tag{3.10}$$

where the first term represents the shift between the measurement temperature T^* and the reference temperature T_s, and the second term represents the shift described above in Eq. 3.9, between the desired temperature T and the reference temperature T_s.

Table 3.1 gives an overview of the temperature differences between the glass transition or melting temperature and the processing temperatures $T_{process}$ of amorphous and semi-crystalline thermoplastics, respectively.

Table 3.1 Difference between Common Reference Temperatures and Processing Temperatures for Common Thermoplastics

Polymer	T_g / T_m (°C)	$T_{process}$ (°C)	ΔT (K)
Polystyrene	90–100	200–240	100–150
High density polyethylene	125–135	180–250	45–125
Low density polyethylene	100–110	150–310	40–210
Polypropylene	160–165	200–250	35–90
Polyamide 66	255–265	295–310	30–55
Polycarbonate	140–150	280–320	130–170
Polyvinyl chloride	–70–80	165–200	85–270

Example 3.1 WLF Shift

Compute the temperature shift factors for the given polycarbonate data using the WLF equation.

The shear dependent viscosity data are given for four different temperatures in the processing temperature range: 260, 280, 300 and 320 °C. In Figure 3.3 the logarithmic viscosity is plotted over the logarithmic shear rate. Calculate the temperature shift factors a_T for every single curve using T_s = 320 °C.

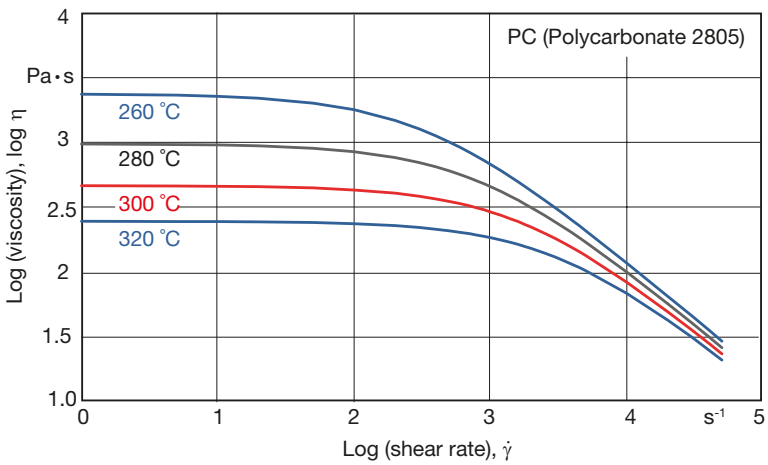

Figure 3.3 Viscosity curves for a polycarbonate

Table 3.2 Logarithmic Zero Shear (0 s^{-1}) and Shear Dependent (2, 3.5 s^{-1}) Viscosity for Different Temperatures

Log shear rate (s^{-1})	logη (260 °C)	logη (280 °C)	logη (300 °C)	logη (320 °C)
0	3.371	2.988	2.666	2.392
2	3.252	2.929	2.634	2.374
3.5	2.495	2.387	2.259	2.116

The shift factors are calculated with the zero shear viscosity data of Table 3.2 using Eq. 3.9. The results are given in Table 3.3:

Table 3.3 Shift Factors and ΔT

T (°C)	$\Delta T = T - T_s = (T - 320\ °C)$	$\log a_T$ (@ 1 s^{-1})	$[-(T - T_s)] / \log a_T$
260	−60	1.409	42.583
280	−40	1.249	32.026
300	−20	1.115	17.937
320	0	1	0

Now plot the WLF diagram using these shift factors with $\left[-\left(T - T_s\right)\right] / \log a_T$ as the y-axis and $\left(T - T_s\right)$ as the x-axis.

The determined linear equation $Y = -0.709\ \Delta T + 1.861$ can be used to calculate the viscosity at any temperature above T_g.

In order to calculate the viscosity at a processing temperature of, e.g., $T = 272$ °C, the temperature difference $\Delta T = 272\ °C - 320\ °C = -48\ °C$ is needed. Therefore, solving the equation yields a Y-value

$$Y = -0.709 \cdot \left(-48\right) + 1.861 = 35.893$$

Together with the temperature difference ΔT, the shift factor can be calculated using

$$\log a_T = \frac{-T - T_0}{Y} = \frac{48}{35.893} = 1.337$$

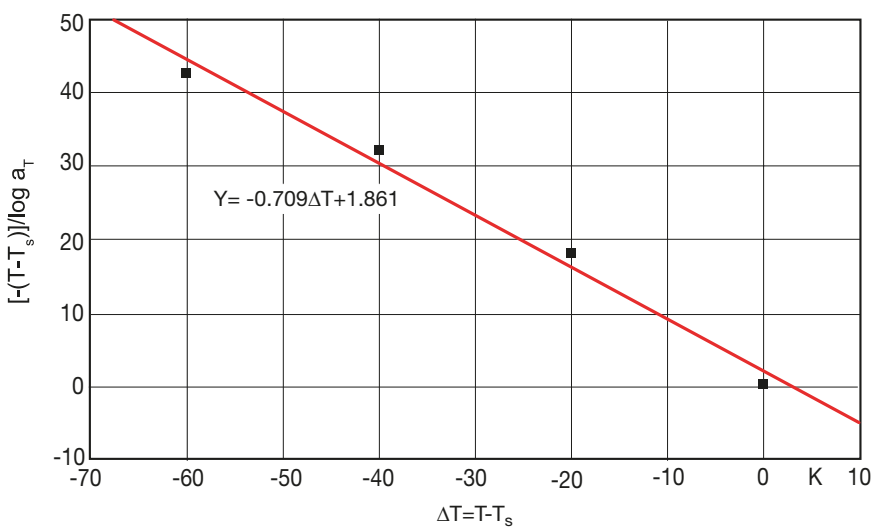

Figure 3.4 WLF diagram for linear regression to determine the constants C_1 and C_2

Now the $\log\eta$ at 272 °C can be obtained by adding the $\log\eta$ at the reference temperature, 320 °C,

$$\log\eta(272\ ^\circ\mathrm{C}) = \log a_T + \log\eta(320\ ^\circ\mathrm{C}) = 1.337 + 2.392 = 3.729$$

The viscosity is calculated as

$$\eta(272\ ^\circ\mathrm{C}) = 10^{3.729} = 5357\ \mathrm{Pa\ s}$$

3.2 Viscous Flow Models

Several models that comply with the *Generalized Newtonian Fluid* assumptions have been proposed in the literature. They vary in their form and in the number of parameters required to fit them to experimental results. These models have two general purposes: to obtain analytical solutions for different flow scenarios encountered in polymer processing, and to allow storage of the measured data with a minimum number of parameters [6]. The flow behavior of different fluids requires usage of different models; some fluids may be shear thinning, others may be fluids that experience a yield stress, and exhibit both behaviors (Fig. 3.5).

A rheologist's task is to find the model, represented in Eq. 3.1, that best fits the measured viscosity data, and at the same time is appropriate for the specific application (process) and type of flow. Complex models that better represent the rheological behavior of the polymer can add significant difficulty to the analysis of a flow field.

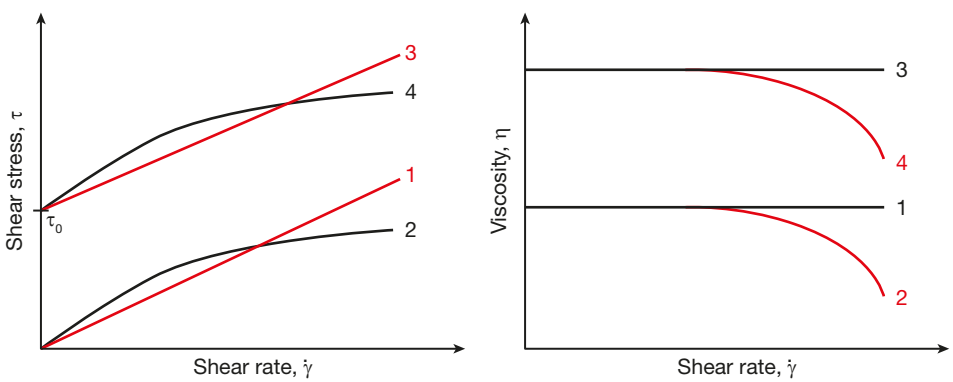

Figure 3.5 Stress curves (left) and viscosity curves (right) for different fluids; (1) Newtonian fluid, (2) shear thinning fluid, (3) Newtonian fluid with yield stress τ_0, (4) shear thinning fluid with yield stress τ_0

However, such models also increase the accuracy of the results and will require numerical solutions. Some of the models used on a day-to-day basis to represent the viscosity of industrial polymers are presented in the following sections.

3.2.1 The Power Law Model

The Power Law model proposed by Ostwald [7] and de Waele [8] is a simple model that accurately represents the shear thinning region in the viscosity versus shear rate curve, but neglects the Newtonian plateau observed at small strain rates, see Fig. 3.6. The Power Law model can be written as:

$$\eta = m(T)\,\dot{\gamma}^{n-1} \tag{3.11}$$

where m is often referred to as the consistency index and n as the Power Law or flow index. The Power Law index represents the shear thinning behavior of the polymer melt for $n < 1$. The consistency index may include the temperature dependence of the viscosity such as represented in Eq. 3.7. The temperature dependence of the consistency index can be represented using the relations given in Section 3.1. For example, one can use

$$m(T) = m_0 \cdot \exp\left[-a\left(T - T_0\right)\right] \tag{3.12}$$

where a is the temperature dependence or sensitivity parameter.

Figure 3.7 presents normalized velocity distributions inside a tube for fluids with various Power Law indices calculated using the Power Law model. It can be seen that a Power Law index of $n = 1$ represents Newtonian behavior and $n = 0$ represents plug flow.

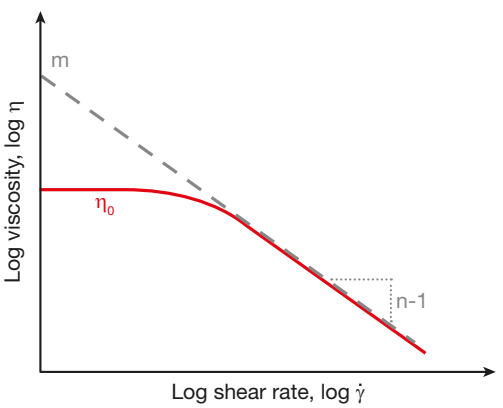

Figure 3.6 Viscosity curve (solid line) and approximation by the Power Law model (dashed line) in Eq. 3.11

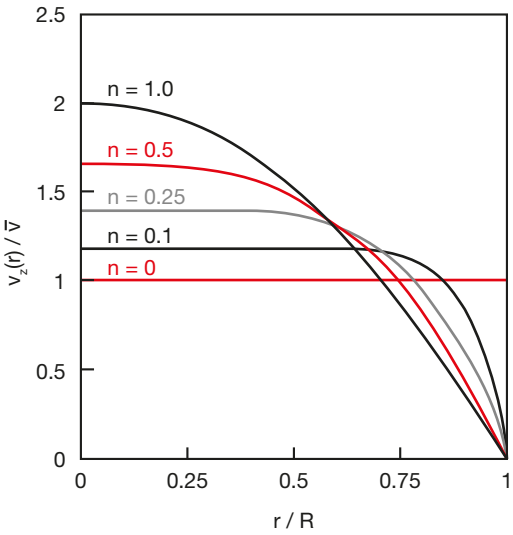

Figure 3.7 Pressure flow velocity distributions inside a tube for fluids with various Power Law indices

Table 3.4 Power Law *n*, Consistency Indices *m*, and Temperature Dependence Constants *a* for Common Thermoplastics

Polymer	m (Pa·s^n)	n	a (°C^{-1})	T (°C)
Polystyrene	2.80×10^4	0.28	−0.025	170
High density polyethylene	2.00×10^4	0.41	−0.002	180
Low density polyethylene	6.00×10^3	0.39	−0.013	160
Polypropylene	7.50×10^3	0.38	−0.004	200
Polyamide 66	6.00×10^2	0.66	−0.016	290
Polycarbonate	6.00×10^2	0.98	−0.015	300
Polyvinyl chloride	1.70×10^4	0.26	−0.019	180

Table 3.4 presents a list of typical Power Law and consistency indices as well as temperature dependence parameters for common thermoplastics. These parameters will vary significantly from grade to grade of the same type of polymer because of the variations in molecular weight, side groups, as well as flowing agents and other processing additives, to name a few. Therefore, the coefficients presented here should be used only as a guideline, and are not recommended for design purposes.

The Power Law model has the following limits:

$$\eta \to 0 \quad \text{as} \quad \dot{\gamma} \to \infty \quad \text{and}$$
$$\eta \to \infty \quad \text{as} \quad \dot{\gamma} \to 0$$

The infinite viscosity at zero strain rate $\dot{\gamma}$ leads to an erroneous result when a region of zero shear rate is encountered, e.g., for flow in a tube or slit. Here, the shear rate

is high at the walls, but low near the center and zero at the center itself. Neglecting the zero shear viscosity values in the center would result in an over-prediction of the viscosity in this area. Therefore, the predicted velocity distribution would be flatter at the center than the experimental profile.

Another example is the filling of a cavity at high flow rates in the beginning of the filling process and at a low flow rate towards the end of filling. Here, the viscosity at the end of filling would be too high, leading to over-predicted injection molding pressure requirements.

Computer simulation of polymer flows overcome this problem by using a truncated model, such as

$$\eta = m_0(T)\,\dot{\gamma}^{n-1} \quad \text{for} \quad \dot{\gamma} > \dot{\gamma}_0 \quad \text{and} \tag{3.13}$$

$$\eta = m_0(T) \quad \text{for} \quad \dot{\gamma} \le \dot{\gamma}_0 \tag{3.14}$$

where m_0 represents a zero shear rate viscosity and $\dot{\gamma}_0$ the shear rate where the Newtonian plateau ends and shear thinning starts to manifest itself.

3.2.2 The Bird-Carreau-Yasuda Model

Bird, Carreau [9] and Yasuda [10] developed a model that accounts for the observed Newtonian plateaus and fits a wide range of strain rates; it contains five parameters:

$$\frac{\eta_{\dot{\gamma}} - \eta_\infty}{\eta_0 - \eta_\infty} = \left(1 + \left|\lambda\dot{\gamma}\right|^a\right)^{\frac{(n-1)}{a}} \tag{3.15}$$

where η_0 is the zero shear rate viscosity, η_∞ is an infinite shear rate viscosity of the second Newtonian plateau, λ is a time constant, and n is the Power Law index, which accounts for the shear thinning behavior, see Fig. 3.8. The parameter a accounts for the width of the transition region between the zero shear viscosity and the Power Law region, which in the original Bird-Carreau model equaled 2. In the literature this model is referred to by different combinations of the collaborators' names, although Carreau model and Bird-Carreau model are commonly used.

In many cases, the infinite shear rate viscosity is negligible, reducing Eq. 3.15 to a three-parameter model:

$$\eta(\dot{\gamma}) = \frac{\eta_0}{\left(1 + \left|\lambda\dot{\gamma}\right|^a\right)^{\frac{(n-1)}{a}}} \tag{3.16}$$

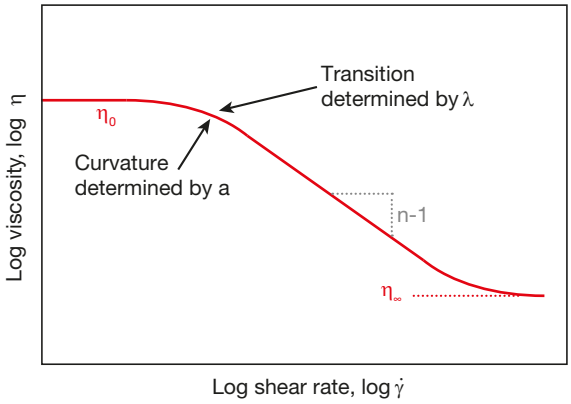

Figure 3.8 Viscosity approximation using the Bird-Carreau-Yasuda model in Eq. 3.15

Equation 3.16 was modified by Menges, Wortberg, and Michaeli [11] to include a temperature dependence using a WLF relation. The modified model, which is often used in commercial polymer data bases, is written as

$$\eta = \frac{k_1 \cdot a_T}{\left(1 + k_2 \dot{\gamma} a_T\right)^{k_3}} \tag{3.17}$$

where the shift factor a_T applies well for amorphous thermoplastics and is written as

$$\log a_T = \frac{8.86\left(k_4 - k_5\right)}{101.6 + k_4 - k_5} - \frac{8.86\left(T - k_5\right)}{101.6 + T - k_5} \tag{3.18}$$

The above equation is comparable to Eq. 3.10 and for semi-crystalline thermoplastics with the Arrhenius shift given in Eq. 3.8.

Table 3.5 presents constants for the Carreau-WLF (amorphous) and Carreau-Arrhenius models (semi-crystalline) for various common thermoplastics.

Table 3.5 Constants for Carreau-WLF (Amorphous) and Carreau-Arrhenius (Semi-Crystalline) Models for Various Common Thermoplastics

Polymer	k_1 (Pa s)	k_2 (s)	k_3	k_4 (°C)	k_5 (°C)	T_0 (°C)	E_0 (J/mol)
Polystyrene	1777	0.064	0.73	200	123	–	–
High density polyethylene	24198	1.38	0.60	–	–	200	22272
Low density polyethylene	317	0.015	0.61	–	–	189	43694
Polypropylene	1386	0.091	0.68	–	–	220	427198
Polyamide 66	44	0.00059	0.40	–	–	300	123058
Polycarbonate	305	0.00046	0.48	320	153	–	–
Polyvinyl chloride	1786	0.054	0.73	185	88	–	–

3.2.3 The Cross-WLF Model

This 6-parameter model considers the effects of shear rate and temperature on the viscosity. Similar to the Bird-Carreau model, this model describes both Newtonian and shear thinning behavior. The shear thinning part is modeled by the general Cross equation [12], which is a popular and earlier alternative to the Bird-Carreau-Yasuda model:

$$\frac{\eta_{\dot{\gamma}} - \eta_{\infty}}{\eta_0 - \eta_{\infty}} = \frac{1}{1 + \left(K \cdot \dot{\gamma}\right)^{1-n}} \tag{3.19}$$

where η_0 is the zero shear rate viscosity, η_{∞} is an infinite shear rate viscosity, K is a time constant such as k_2 in Table 3.5, and n is the Power Law index, which accounts for the shear thinning behavior. For $\eta_{\dot{\gamma}} \ll \eta_0$ and $\eta_{\dot{\gamma}} \gg \eta_{\infty}$, the Cross model reduces to the Power Law model. If the infinite shear rate viscosity is negligible, the well-known form of the Cross model can be written as

$$\eta\left(\dot{\gamma}\right) = \frac{\eta_0}{1 + \left(\frac{\eta_0 \dot{\gamma}}{\tau^*}\right)^{1-n}} \tag{3.20}$$

Here, τ^* is the critical shear stress at the transition from the Newtonian plateau, with $K = \eta_0 / \tau^*$, and n is the Power Law index, see Fig. 3.9. If the model is used to fit the data prior to making the Weissenberg-Rabinowitsch correction (see Eq. 6.19 in Chapter 6), the apparent shear stress can be shifted [13] by setting

$$\tau^* = \left(\frac{4n}{3n+1}\right)^{\frac{n}{1-n}} \tag{3.21}$$

In this case, the remaining model parameters remain unchanged.

The zero shear viscosity is modeled with the WLF equation

$$\eta_0\left(T\right) = D_1 \cdot \exp\left[\frac{A_1\left(T - D_2\right)}{A_2 + T - D_2}\right] \tag{3.22}$$

where D_1 is the viscosity at a reference temperature D_2 and A_1 and A_2 describe the temperature dependency, which is comparable to the temperature shift factor described in Eq. 3.9.

The Cross-WLF model is the most common model used by injection molding simulation software, because it offers the best fit to most viscosity data [14]. Table 3.6 presents constants for various common thermoplastics.

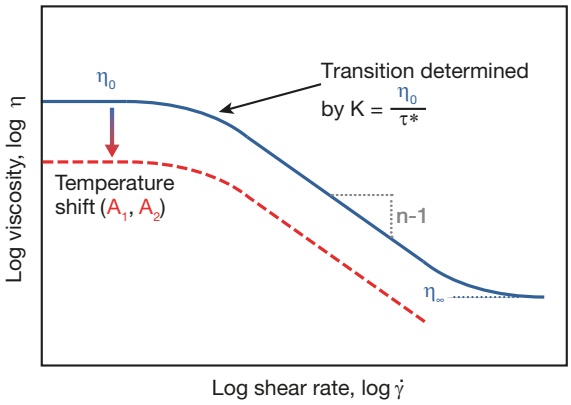

Figure 3.9 Viscosity approximation with the Cross-WLF model in Eq. 3.20 and Eq. 3.22

Table 3.6 Constants for the Cross-WLF Model for Various Common Thermoplastics [15, 16]

Polymer	τ (Pa)	n	D_1 (Pa s)	D_2 (K)	A_1	A_2 (K)
Polystyrene	31,200	0.243	1223	503	6.5	158.2
High density polyethylene	75,700	0.342	7×10^{12}	153	26.3	51.6
Low density polyethylene	34,515	0.315	3.1×10^{14}	233	34.6	51.6
Polypropylene	32,477	0.251	564	493	2803.3	165,097.1
Polyamide 66	151,905	0.347	144	573	256,999.6	11,235,949
Polycarbonate	8,437,056	0.116	462	573	8.4	246.8
Polyvinyl chloride	46,070	0.399	3.2×10^{16}	353	42.9	51.6

3.2.4 The Bingham Model

The Bingham model is an empirical two-parameter model that represents the rheological behavior of materials that exhibit yield stresses τ_0, below which the material does not flow. Typical examples of Bingham fluids are polymer emulsions and slurries. In the flow range, above the yield stress, a Bingham fluid behaves like a Newtonian liquid and can therefore be represented as

$$\eta = \infty \quad \text{or} \quad \dot{\gamma} = 0 \quad \text{for} \quad \tau \leq \tau_0 \tag{3.23}$$

$$\eta = \mu_0 + \frac{\tau_0}{\dot{\gamma}} \quad \text{for} \quad \tau > \tau_0 \tag{3.24}$$

Here, τ is the magnitude of the deviatoric stress tensor and μ_0 is the Newtonian viscosity for vanishing yield stress. The model shows that a critical level of stress must be attained in order to initiate flow.

3.2.5 The Herschel-Bulkley Model

The Herschel-Bulkley model is widely used to represent the behavior of fluids that have a yield stress, such as the Bingham fluid, but that otherwise exhibit shear thinning behavior. The model is represented as

$$\tau = \tau_0 + m \cdot \dot{\gamma}^n \tag{3.25}$$

$$\eta = \frac{\tau_0}{\dot{\gamma}} + m \cdot \dot{\gamma}^{n-1} \quad \text{for} \quad \tau > \tau_0 \tag{3.26}$$

where τ_0 is the yield stress, m the consistency index, and n the Power Law or flow index. As with the Bingham model, this model also requires that a critical level of stress must be attained to initiate flow. Below this critical stress τ_0, the material behaves like a solid, allowing it to sustain stress without flow, but above the critical stress, the material flows like a Power Law fluid. Similar to the Power Law model, $n < 1$ represents shear thinning, $n > 1$ shear thickening, and $n = 1$ reduces the model to the Bingham model and represents Newtonian flow above the critical yield stress.

Table 3.7 shows that all models discussed so far can be derived from one base equation. While the Power Law model is the simplest model that can be used when the shear rate is high, the Cross-WLF model is the most common model in numerical simulations because it fits the viscosity data of a wide range of materials. In terms of practical applications, it is closely followed by the Bird-Carreau-Yasuda model.

Table 3.7 Overview of Viscous Flow Models

	Power Law	Bird-Carreau-Yasuda	Cross-WLF	Bingham
Base equation		$\frac{\eta - \eta_\infty}{\eta_0 - \eta_\infty} = \frac{1}{\left[1 + \left(K\dot{\gamma}\right)^a\right]^{\frac{(1-n)}{a}}}$		
Assumptions	$\eta \ll \eta_0$, $\eta \gg \eta_\infty$, $\eta_\infty = 0$, $a = 1$, $K = m$	$\eta_\infty = 0$, $K = \lambda$	$\eta_\infty = 0$, $a = 1$, $K = \frac{\eta_0}{\tau^*}$	$\eta \ll \eta_0$, $\eta \ll \mu_0$, $K = \tau_Y$, $n = 0$
Model	$\eta = m \cdot \dot{\gamma}^{n-1}$	$\eta = \frac{\eta_0}{\left(1 + \lvert\lambda\dot{\gamma}\rvert^a\right)^{\frac{(1-n)}{a}}}$	$\eta = \frac{\eta_0}{1 + \left(\frac{\eta_0 \dot{\gamma}}{\tau^*}\right)^{1-n}}$	$\eta = \mu_0 + \frac{\tau_Y}{\dot{\gamma}}$

3.2.6 Accounting for Pressure Dependence in Viscous Flow Models

Although the effect of pressure on viscosity is well known, few research groups have focused on this topic. However, using some experimental values in conjunction with theoretical considerations, pressure effects have been incorporated into existing models. These are discussed in the following sections.

3.2.6.1 Power Law

The Power Law model, Eq. 3.11, may also include a dimensionless temperature sensitivity factor, a or α, Eq. 3.7, as well as a dimensionless pressure sensitivity factor, b or β, proposed by Barus [17], respectively,

$$\eta(T,\dot{\gamma},p) = m_0 \cdot \exp\left[-a(T-T)_0\right] \cdot \exp\left[b\left(p-p_0\right)\right] \cdot \dot{\gamma}^{n-1} \tag{3.27}$$

The opposing signs of the sensitivity factors a and b reflect their effect on viscosity, due to the fact that viscosity increases with decreasing temperature and increasing pressure. The terms in the above equation can be expressed in terms of a temperature shift factor

$$a_T\left(T\right) = \frac{\eta_0\left(T\right)}{\eta_0\left(T_0\right)} = \exp\left[-a\left(T-T_0\right)\right] \tag{3.28}$$

and a pressure shift factor

$$a_p\left(p\right) = \frac{\eta_0\left(p\right)}{\eta_0\left(p_0\right)} = \exp\left[b\left(p-p_0\right)\right] \tag{3.29}$$

This model neglects the Newtonian plateau, or shear independent behavior, observed with polymers at low shear rates. However, the exponential form of the viscosity shifts make it easy to represent the sensitivity to temperature and pressure during measurements and processing.

3.2.6.2 Carreau-WLF

Cogswell [18] related a viscosity change to a change in density, because a temperature reduction and an increase in pressure will increase both density and viscosity. Based on this assumption, Menges et al. [11] introduced the pressure shift in the WLF-temperature shift, Eq. 3.10, in combination with the Bird-Carreau-Yasuda model, Eq. 3.17. For their shift $T_s\left(p\right)$ they used the glass transition temperature T_g from pressure-volume-temperature (pvT) measurements [19, 20] at 1 bar, and a correction that included the pressure dependence of T_g

$$T_s(p) = T_g + 43\,\mathrm{K} = T_{g\,(1\,\mathrm{bar})} + (P_1 \cdot p) + 43\,\mathrm{K} \tag{3.30}$$

with P_1 being the pressure dependence of the glass transition and p the absolute pressure. P_1 ranges from 0.02 to 0.03 K/bar, depending on the polymer. Introducing Eq. 3.30 into Eq. 3.18 results in

$$\log \eta(T,p) = \log \eta_0 + \frac{8.86\,(T^* - T_s)}{101.6 + T^* - T_s} - \frac{8.86\,(T - T_s - P_1 \cdot p)}{101.6 + T - T_s - P_1 \cdot p} \tag{3.31}$$

In the above equation, the first term represents a shift between the measured temperature T^* and the reference temperature T_s. The second term represents the temperature and pressure shifts between the actual temperature and the reference temperature, as well as between 1 bar and the actual pressure. Hence, in the above model a rise in pressure is equivalent to a drop in temperature. Menges et al. [11] proposed that P_1 = 0.02 K/bar, which provides a good approximation in case *pvT*-data are not available.

3.2.6.3 Cross-WLF

Incorporating the pressure dependence in the Cross-WLF equation leaves the shear thinning part unchanged. It is modeled by the general Cross equation

$$\eta(\dot{\gamma}) = \frac{\eta_0}{1 + \left(\frac{\eta_0 \dot{\gamma}}{\tau^*}\right)^{n-1}} \tag{3.20}$$

where τ^* is the critical shear stress at the transition from the Newtonian plateau, η_0, to the Power Law regime, and n denotes the Power Law index.

The zero shear viscosity is modeled with the WLF equation

$$\eta_0(T,p) = D_1 \cdot \exp\left[\frac{A_1\,(T - T_c)}{A_2 + T - T_c}\right] \tag{3.32}$$

with $T_c = D_2 + D_3 \cdot p$ and $A_2 = \tilde{A}_2 + D_3 \cdot p$. In addition to the parameters in Eq. 3.25, D_3 denotes the pressure dependency, while p is the pressure acting on the melt. Because of the added parameters, the model is sometimes referred to as the 7-parameter model. D_1 reflects the initial level of viscosity at reference conditions, D_2 is typically taken as the glass transition temperature T_g, and A_1 and $\tilde{A}_2$ are temperature dependent factors. Other than P_1 in Eq. 3.31, D_3 also corrects the reference temperature D_2. If pressure dependent viscosity data are not available, *pvT*-data are used to account for the pressure dependence of the glass transition temperature. Equation 3.32 is often written as

$$\eta_0(T,p) = D_1 \cdot \exp\left[\frac{A_1\left(T - D_2 - D_3 \cdot p\right)}{\tilde{A}_2 + T - D_2}\right] \tag{3.33}$$

Typical values for the pressure sensitivity for different polymers are listed in Table 3.8.

Table 3.8 Pressure Shift Factors of Viscosity for Various Common Polymers

Polymer	b or β (bar^{-1}) Power Law	Reference	D_3 (K bar^{-1}) Cross-WLF	Reference
Polystyrene	0.004345 0.00568, 0.0029	21, 22, 23	0.1	24
High density polyethylene	0.001036 0.0015, 0.001 0.001	21, 22, 23 25	0.012	26
Low density polyethylene	0.00183 0.00147 0.00165, 0.0016	21, 23, 25		
Polypropylene	0.002091, 0.00282, 0.0022 0.0023	21, 22, 23, 25	0.0205, 0.014	24, 27
Polycarbonate	0.003112	21	0.03, 0.018	26, 27
Polymethyl methacrylate	0.004357 0.0024	21, 23	0.023	14

The differences between the shift factors for one material reported by different research groups underline the difficulty of the measurement. Therefore, different measurement methods for the pressure influence on viscosity are described in more detail in Chapter 6.

3.2.6.4 Universal Temperature and Pressure Invariant Viscosity Function

Because the viscosity behavior of a specific thermoplastic is very similar from grade to grade one can predict its full behavior based on one single function. This allows the use of single point data, such as measured with an MFI, to predict the viscosity of a given material as a function of pressure and temperature. This "universal" behavior was recognized in the early polymer research days and is reflected in the WLF shift. Different research groups have investigated this temperature and pressure invariant representation of viscosity [28, 29, 30, 31, 32, 33]. Reference viscosity curves, such as the one presented for polycarbonate in Fig. 3.10, can then be used as a reference, if no multipoint data are available. To generate such a curve, the shear dependent viscosity is divided by the shear independent viscosity, η_0, for each given temperature and pressure. This is followed by multiplying the shear rate by η_0. By doing this, the "universal" curve approaches a slope of −1, or a 45° angle in a log-log scale.

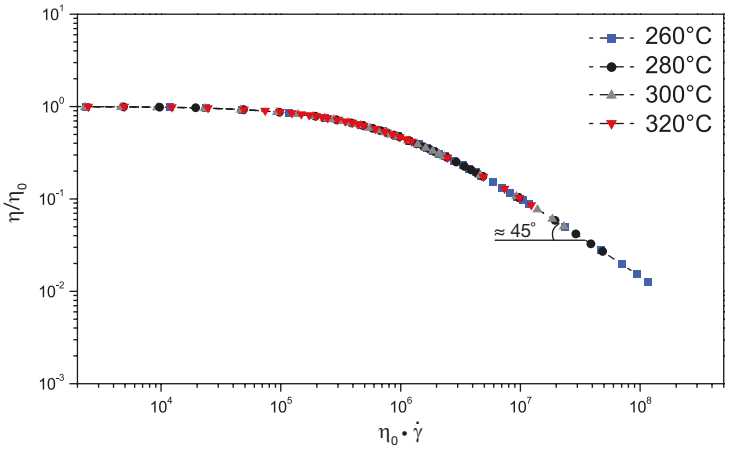

Figure 3.10 Master curve for polycarbonate (Makrolon 2805) as obtained as a function of zero shear viscosity

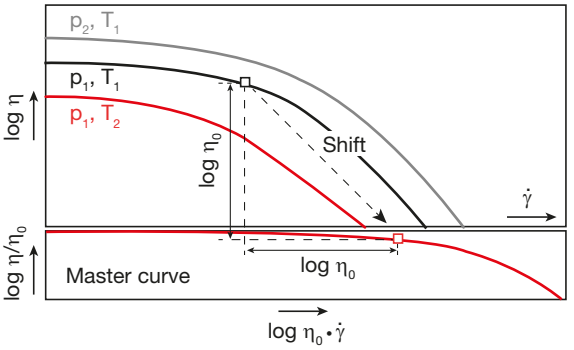

Figure 3.11 Measured viscosity at different temperatures and pressures as a function of shear rate and shift into general viscosity function (master curve)

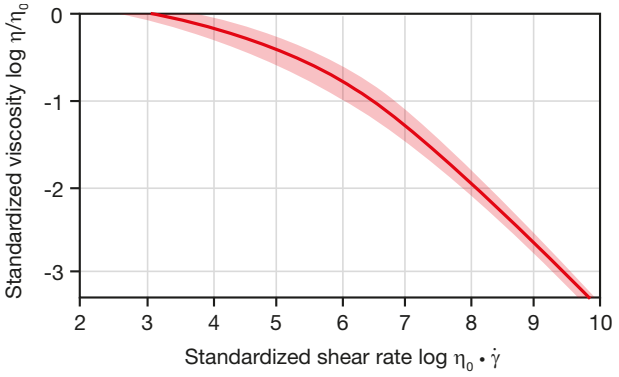

Figure 3.12 Universal temperature-independent viscosity characteristic of polymer melts

Vinogradov and Malkin [34] discovered that the viscosity curves for several structurally different materials, such as polyethylene, polypropylene, polystyrene, and unvulcanized natural rubber, could be reduced to a narrow band of viscosity curves if plotted as $\log \eta/\eta_0 = f\left(\eta_0 \cdot \dot{\gamma}\right)$ as shown in Fig. 3.12.

Figure 3.11 shows schematically how the master curve is generated from shear dependent viscosity data.

Dividing the viscosity by the zero shear viscosity gives a dimensionless number, $\log \eta/\eta_0$, which becomes zero when the viscosity approaches the shear independent viscosity at the Newtonian plateau, and is negative in the shear thinning region, see Fig. 3.12.

The centerline in Fig. 3.12 represents the universal, temperature invariant viscosity function or master curve. The band width shows how close the master curves align for the investigated materials [34]. As the pressure dependence can be converted into a temperature dependence, this master curve can also be used for a pressure and temperature independent presentation [35]. The master curve can be described by a general viscosity function in the form

$$\eta\left(\dot{\gamma},T,p\right) = \eta_0 \left[1 + A_1 \left(\eta_0 \, \dot{\gamma}\right)^{\alpha} + A_2 \left(\eta_0 \, \dot{\gamma}\right)^{2\alpha}\right]^{-1} \tag{3.34}$$

where η_0 is the zero shear viscosity as a function of temperature and pressure as well as shear rate $\dot{\gamma}$. A_1, A_2 and α are constants with $A_1 = 6.12 \cdot 10^{-3}$, $A_2 = 2.85 \cdot 10^{-4}$, and $\alpha = 0.355$ [34]. Rewriting the constants $\tau_1 = A_1^{-1/\alpha}$ and $\tau_2 = A_2^{-1/2\alpha}$ and assuming $\alpha = n - 1$, a function very similar to the Cross model, Eq. 3.20, is obtained

$$\eta\left(\dot{\gamma},T,p\right) = \frac{\eta_0}{1 + \left(\dfrac{\eta_0 \, \dot{\gamma}}{\tau_1}\right)^{\alpha} + \left(\dfrac{\eta_0 \, \dot{\gamma}}{\tau_2}\right)^{2\alpha}} \tag{3.35}$$

where $\tau_1 = 1{,}715{,}943$ Pa and $\tau_2 = 98{,}441$ Pa. Menges et al. [35] showed that this universal viscosity function allows the use of single-point viscosity data to predict rate dependent flow behavior. Of course, the use of multi-point data is always recommended. However, in case only single-point data such as MFI is available, this approach can be used to estimate the shear rate dependent behavior. An example for this estimation is given in the following.

Example 3.2 Vinogradov's Universal Viscosity Approach

For injection molding experiments with HDPE, the following single-point material properties are known from the material datasheet:

- MFI: 20 g/10 min measured at 190 °C and 2.16 kg weight
- Density at room temperature ρ_{T_0}: 0.948 g/cm^3
- Linear thermal expansion coefficient α: $6.9 \cdot 10^{-4}$ K^{-1}

In order to obtain shear dependent viscosity data, the single-point MFI value can be used. For this approach the testing conditions and geometry of the die must also be known. For MFI data, the geometry of the ASTM standard D1234 [36] can be used; the standard utilizes a capillary with 2.095 mm diameter (R = 1.0475 mm) and 8 mm length.

The melt flow index (MFI) is converted into the melt volume flow rate (MVR) Q by

$$Q = \mathrm{MVR} = \frac{\mathrm{MFI}}{\rho(T^*)} = \frac{20\ \mathrm{g \cdot cm^3}}{0.704\ \mathrm{g \cdot 10\ min}} = 28.39\ \frac{\mathrm{cm^3}}{10\ \mathrm{min}}$$

where the density ρ at the measurement temperature T^* of 190 °C is calculated by

$$\rho(T) = \rho_{T_0}\ \frac{1}{1+\alpha\left(T^* - T_0\right)} = 0.948\ \frac{\mathrm{g}}{\mathrm{cm^3}} \cdot \frac{1}{1+3 \cdot 6.9 \cdot 10^{-4}\ \mathrm{K^{-1}}\left(190\ ^\circ\mathrm{C} - 23\ ^\circ\mathrm{C}\right)}$$

$$= 0.704\ \frac{\mathrm{g}}{\mathrm{cm^3}}$$

where T_0 is room temperature, and α is the linear thermal expansion coefficient, which has to be multiplied by 3 to obtain the required volume expansion coefficient.

Because the flow within the capillary can be represented by the Hagen-Poiseuille equation (Chapter 4), the shear rate at the wall of the capillary can be easily calculated. Using Schümmer's assumption [37], which is explained in more detail in Section 6.4.2, that the intersection of the velocity distribution of the Newtonian and the shear thinning fluid coincides at the same position for all polymers, the true shear rate $\dot{\gamma}_\mathrm{w}$ (Eq. 6.28) and shear stress τ_w (Eq. 6.29) at the wall can be computed for the melt flow indexer measurement using

$$\dot{\gamma}_\mathrm{w} = \frac{Q}{R^3} = \frac{28.39\ \mathrm{cm^3}}{\left(0.10475\ \mathrm{cm}\right)^3 \cdot 600\ \mathrm{s}} = 41.17\ \mathrm{s^{-1}}$$

and

$$\tau_\mathrm{w} = \frac{R \cdot \pi \cdot \partial p/\partial z}{8} = \frac{0.0010475\ \mathrm{m} \cdot \pi \cdot 768.12\ \mathrm{MPa}}{8 \cdot \mathrm{m}} = 0.32\ \mathrm{MPa}$$

where $\partial p/\partial z$ is the pressure gradient along the capillary over the length L, given by

$$\partial p/\partial z = \frac{F}{R^2 \cdot \pi \cdot L} = \frac{21.18\ \mathrm{N}}{\left(0.0010475\ \mathrm{m}\right)^2 \cdot \pi \cdot 0.008\ \mathrm{m}} = 768.12\ \frac{\mathrm{MPa}}{\mathrm{m}}$$

where F is the piston load of the MFI (2.16 kg · 9.81 m/s^2) and L is the die length. The radius of the piston should be used for the pressure calculation; however, for simplification the radius of the die R is used here.

The viscosity under MFI measurement conditions is then

$$\eta\left(\dot{\gamma}_w, T^*, p^*\right) = \frac{\tau_w}{\dot{\gamma}_w} = \frac{0.32\ \text{MPa}}{41.17\ \text{s}^{-1}} = 7675.15\ \text{Pa s}$$

Because the shear rate experienced by the material inside the melt flow indexer is very small (< 100 s^{-1}), the resulting viscosity value of 7,675.15 Pa s can be considered as the zero shear viscosity $\eta_0\left(T^*, p^*\right)$. To assure that this assumption is correct, the MFI should be measured using small loads, allowing the presented calculation of $\dot{\gamma}_w$ and τ_w.

In order to obtain the zero shear viscosity at a given temperature and pressure, first the pressure at the entrance of the MFI measurement die, p^*, has to be calculated using

$$p^* = \frac{\partial p/\partial z \cdot L}{2} = \frac{768.12\ \text{MPa} \cdot 0.008\ \text{m}}{2 \cdot \text{m}} = 3.07\ \text{MPa} = 30.72\ \text{bar}$$

Now the viscosity under typical processing conditions of HDPE, e.g., 210 °C at 1 bar and at 1000 bar, should be measured. Therefore, the temperature and pressure shifts of the modified Carreau-WLF model, Eq. 3.31, have to be used

$$\eta_0\left(T,p\right) = \eta_0\left(T^*,p^*\right) \cdot 10^{\frac{8.86\left(T^*-T_s\right)}{101.6+T^*-T_s} - \frac{8.86\left(T-T_s+P_1 \cdot p\right)}{101.6+T-T_s+P_1 \cdot p}}$$

where T^* = 190 °C, p^* = 30.72 bar, and P_1 = 0.02 K/bar. For T = 210 °C, p = 1 bar and T_s = −150 °C + 43 °C = −107 °C. The zero shear viscosity is

$$\begin{aligned}\eta_0\left(T,p\right) &= \eta_0\left(T^*,p^*\right) \cdot 10^{\frac{8.86\left(190\,^\circ\text{C}+107\,^\circ\text{C}\right)}{101.6\,^\circ\text{C}+190\,^\circ\text{C}+107\,^\circ\text{C}} - \frac{8.86\left(210\,^\circ\text{C}+107\,^\circ\text{C}+0.61\,^\circ\text{C}\right)}{101.6\,^\circ\text{C}+210\,^\circ\text{C}+107\,^\circ\text{C}+0.61\,^\circ\text{C}}} \\ &= 7675.15\ \text{Pa s} \cdot 10^{-0.111029} = 5943.72\ \text{Pa s}\end{aligned}$$

For T = 210 °C, p = 1000 bar and T_s = −150 °C + 43 °C = −107 °C, the zero shear viscosity is

$$\begin{aligned}\eta_0\left(T,p\right) &= \eta_0\left(T,1000\ \text{bar}\right) \cdot 10^{\frac{8.86\left(210\,^\circ\text{C}+107\,^\circ\text{C}\right)}{101.6\,^\circ\text{C}+210\,^\circ\text{C}+107\,^\circ\text{C}} - \frac{8.86\left(210\,^\circ\text{C}+107\,^\circ\text{C}-20\,^\circ\text{C}\right)}{101.6\,^\circ\text{C}+210\,^\circ\text{C}+107\,^\circ\text{C}-20\,^\circ\text{C}}} \\ &= 5943.72\ \text{Pa}\ s \cdot 10^{0.1079000} = 7620.05\ \text{Pa s}\end{aligned}$$

In addition, the shear rate dependent viscosity can now be calculated with the universal Eq. 3.34 for T = 210 °C, p_1 = 1 bar, and p_2 = 1000 bar so that the following Table 3.9 can be generated.

Table 3.9 Shear Rate Dependent Viscosity Data of HDPE at 210 °C and 1 and 1000 bar Using the Vinogradov Approach (Eq. 3.34)

Shear rate (s^{-1})	1	40	80	200	400	1000	3000	5000
1 bar	4680	1770	1270	768	507	284	137	97
1000 bar	5820	2260	1620	984	650	364	176	124

3.3 Elongational Viscosity

In polymer processes such as fiber spinning, blow molding, thermoforming, foaming, certain extrusion die flows, and compression molding with specific processing conditions, the major mode of deformation is elongational.

To illustrate elongational flows, consider the fiber spinning process shown in Figure 3.13.

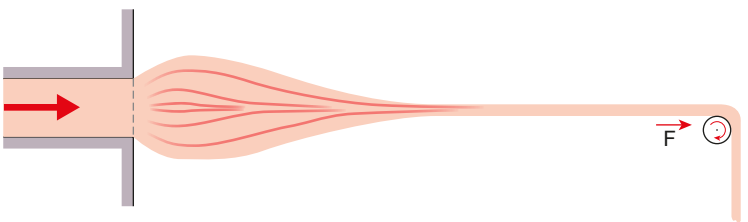

Figure 3.13 Schematic diagram of a fiber spinning process

As the filament is stretched, a simple elongational flow develops with the following components of the rate of deformation:

$$\dot{\gamma}_{11} = -\dot{\varepsilon} \tag{3.36}$$

$$\dot{\gamma}_{22} = -\dot{\varepsilon} \tag{3.37}$$

$$\dot{\gamma}_{33} = -2\dot{\varepsilon} \tag{3.38}$$

where $\dot{\varepsilon}$ is the elongation rate, and the non-diagonal terms of $\dot{\gamma}_{ij}$ are all zero. The diagonal terms of the total stress tensor can be written as

$$\sigma_{11} = -p - \eta\dot{\varepsilon} \tag{3.39}$$

$$\sigma_{22} = -p - \eta\dot{\varepsilon} \tag{3.40}$$

$$\sigma_{33} = -p + 2\eta\dot{\varepsilon} \tag{3.41}$$

Because the only outside forces acting on the fiber are in the axial or 3-direction, for the Newtonian case, σ_{11} and σ_{12} must be zero. Hence,

$$p = -\eta\dot{\varepsilon} \tag{3.42}$$

$$\sigma_{33} = 3\eta\dot{\varepsilon} = \overline{\eta}\dot{\varepsilon} \tag{3.43}$$

which is known as *elongational viscosity or Trouton viscosity* [38]. This is analogous to elasticity with the following relation between elastic modulus, E, and shear modulus, G:

$$\frac{E}{G} = 2(1+\nu) \tag{3.44}$$

where ν is Poisson's ratio. For the incompressibility case, where ν = 0.5, Eq. 3.44 reduces to

$$\frac{E}{G} = 3 \tag{3.45}$$

Figure 3.14 [39] shows shear and elongational viscosities of polystyrene. In the region of the Newtonian plateau, the limit of 3, shown in Eq. 3.43, is quite clear.

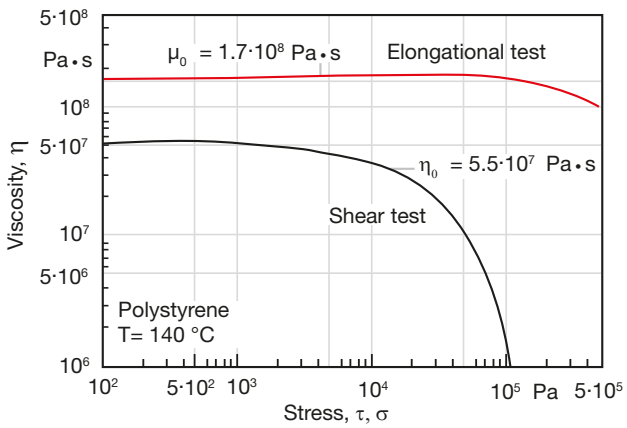

Figure 3.14 Shear and elongational viscosity curves of polystyrene

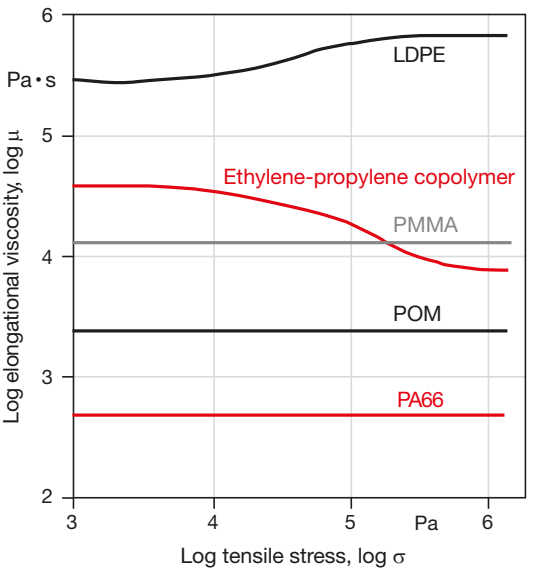

Figure 3.15 Elongational viscosity curves as functions of tensile stress for several thermoplastics

Figure 3.15 [40] shows plots of elongational viscosities at common processing conditions as functions of stress for various thermoplastics. Measuring elongational or extensional viscosity is an extremely difficult task, because maintaining a constant strain rate is challenging. For example, the specimen must be deformed uniformly exponentially. Different common measurement techniques are explained in more detail in Chapter 6 and additional examples are provided.

3.4 Suspension Rheology

Particles suspended in a material, such as in reinforced or filled polymers, have a direct effect on the properties of the final component and on the viscosity during processing. Today, polymer materials are seldom used in their pure form. Instead various filler particles are used to enhance mechanical properties, increase the resistance to wear, improve thermal or electrical conductivity, add magnetic properties, and much more. In addition, the use of polymers as binders during ceramic processing is another growing market. The shape of those particles can vary from rod-like particles in fiber suspensions to spherical particles or flakes. The viscosity of a fluid filled with particles is higher than that of the neat polymer. The viscosity of the filled system depends on the volume fraction of the particles, the particle shape, the average particle size and the size distribution, the shear rate, and the

interaction between particles as well as between particles and the polymer matrix [41]. A volume fraction between 20 to 40% is considered low filler loading range, whereas 40 to 60% is referred to as high filler loading range. The higher the volume fraction and the larger the aspect ratio (fiber > platelet > sphere) of the particle, the higher the viscosity increase compared to the neat polymer.

Depending on whether the matrix system is a thermoplastic or a thermoset, the flow is shear thinning or Newtonian, respectively [42]. However, during flow particles may agglomerate. The shape of these clusters is dependent on the shear rate and directly related to a change in viscosity [43, 44]. Another effect that accompanies agglomeration or filler size in general is thixotropy [43]. During shearing, the initial formation of the particles begins to change until a final structure has formed [45]. This change is accompanied by an initial decrease in viscosity until a steady-state Newtonian plateau is reached. Both effects are directly proportional to the volume fraction and size of the filler.

However, viscosity measurements of filled polymers are more difficult than those of neat polymers, because the no-slip condition at the wall cannot be readily assumed. Furthermore, shearing occurs not only at the wall but also between the particles. For measurements in capillary rheometers, problems occur at the inlet of the die. First, the inlet pressure drop is larger and sometimes instable. Second, phase separation can occur with filled polymers and therefore impede the development of steady flow.

For example, magnetic particles, such as strontium ferrite, distributed in a polymer matrix are used to manufacture permanent magnets. These particles tend to agglomerate, as seen in Fig. 3.16. An extensive study on single-point viscosity values, such as the melt volume rate (MVR) and shear rate and temperature dependent viscosity data, revealed the influence of particle content on flow behavior [46].

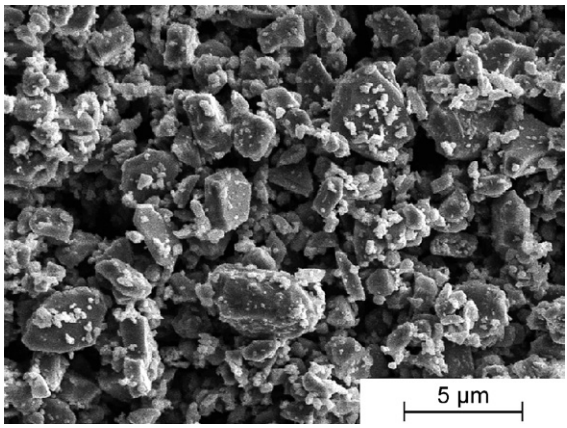

Figure 3.16 SEM of strontium ferrite particles

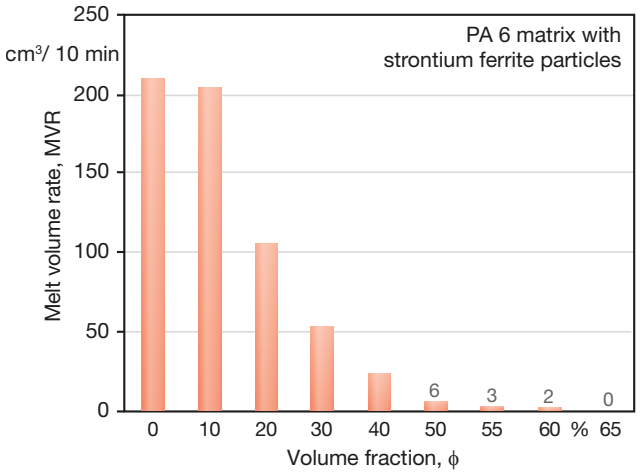

Figure 3.17 Dependence of melt volume rate (MVR) on volume fraction of strontium ferrite in a PA 6 matrix

The influence of different volume fractions of strontium ferrite on the MVR is shown in Fig. 3.17.

Figures 3.18 and 3.19 present the effect of increasing filler volume fraction on the shear rate and temperature dependence, respectively.

The viscosity shifted to higher values with increasing filler content. In the shear rate range from $10^3 - 10^4\ s^{-1}$ the viscosity shifted from 10^2 to $5 \cdot 10^2$ Pa s for neat PA, and to $5 \cdot 10^3$ to 10^4 Pa s for 60 vol.-% filler. Referring to Fig. 3.17, we can see that because of the higher apparent viscosity during the measurements using higher filler

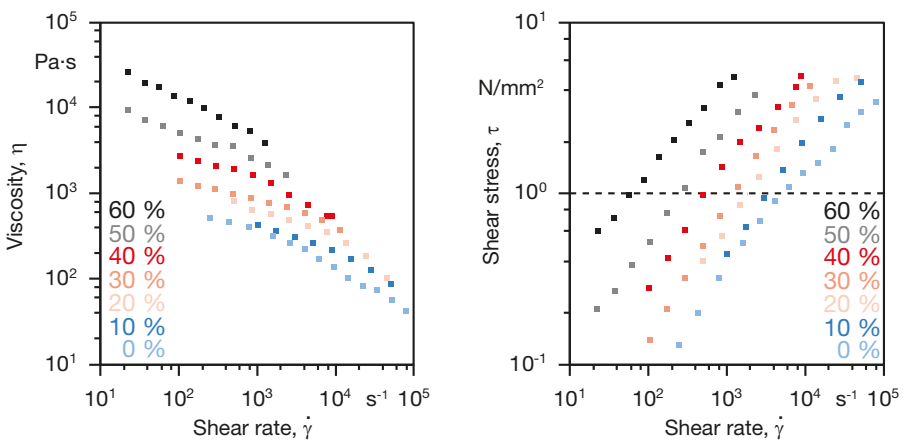

Figure 3.18 Effect of volume fractions of strontium ferrite in PA 6 at 280 °C; Left: shear rate dependent viscosity; Right: shear rate dependent stress

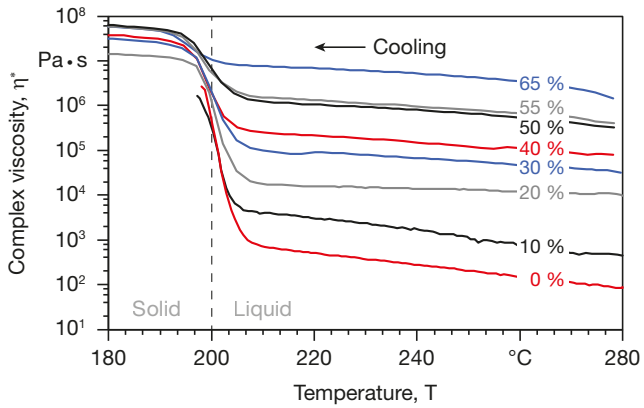

Figure 3.19 Temperature dependence of the complex viscosity of PA 6 filled with strontium ferrite; frequency: 1 Hz, cooling rate: 5 K/min

content, lower shear rates were achieved. A conversion of the shear rate dependent viscosity and the corresponding shear stress shows a linear dependence of the shear stress on the shear rate when plotted on a logarithmic scale. Therefore, only the viscosity level, but not the shear rate dependence is affected by the filler content.

The temperature dependence of the zero shear viscosity is measured in a parallel plate rheometer. The drop once the crystallization temperature is reached decreases with increasing filler content and almost vanishes for 65 vol.-% filler content. Therefore, the influence of filler content is strong in the melt and weaker in the solid material.

Numerous models have been proposed to predict the viscosity of filled liquids [47, 48, 49, 50, 51], and most take the form of a power series of the volume fraction ϕ:

$$\frac{\eta_f}{\eta_0} = 1 + a_1\,\phi + a_2\,\phi^2 + a_3\,\phi^3 + \ldots \tag{3.46}$$

The linear term in Eq. 3.46 represents the reduction of the flow passage caused by the fillers that are dragged by the fluid and are not deformed, as shown in Fig. 3.20.

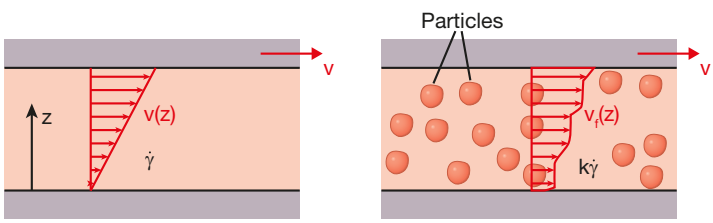

Figure 3.20 Schematic diagram of strain rate increase in a filled system

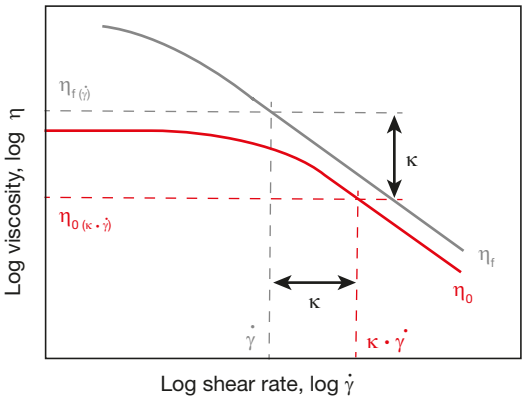

Figure 3.21 Viscosity approximation using the Geisbüsch Model in Eq. 3.49

For instance, Einstein's model for viscosity of a filled liquid only includes the linear term with a_1 = 2.5. He derived his equation based on a viscous dissipation balance. The quadratic term in the equation represents the effects related to the interaction between the filler particles. For small volume fractions (< 10 vol.-%), Eq. 3.46 can be simplified to

$$\frac{\eta_f}{\eta_0} = 1 + \phi^2 \tag{3.47}$$

Geisbüsch suggested a model that included a yield stress, and in which the strain rate of the melt increases by a factor κ as

$$\eta_f(\dot{\gamma}) = \frac{\tau_0}{\dot{\gamma}} + \kappa \cdot \eta_0(\kappa\dot{\gamma}) \tag{3.48}$$

where η_f is the viscosity of the filled polymer, τ_0 is the yield stress, $\dot{\gamma}$ is the shear rate, and η_0 is the viscosity of the neat polymer, see Fig. 3.21. For high deformation stresses, as typically found in polymer processing, the yield stress in the filled polymer melt can be neglected, resulting in the following, simplified expression

$$\eta_f(\dot{\gamma}) \approx \kappa \cdot \eta_0(\kappa\dot{\gamma}) \tag{3.49}$$

Figure 3.22 compares Geisbüsch's experimental data to the results from Eq. 3.46 using the coefficients a_1 = 2.5 and a_2 = 14.1 as derived by Guth [49]. The data and Guth's model seem to agree well. A comprehensive survey of particulate suspensions was given by Gupta [52], and on short-fiber suspensions by Milliken and Powell [53].

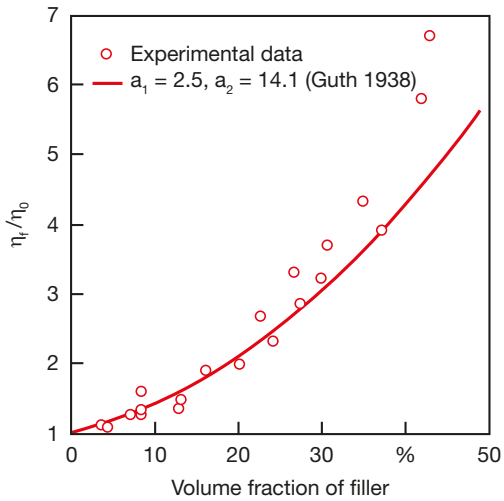

Figure 3.22 Viscosity increase as a function of volume fraction of filler for polystyrene and low density polyethylene containing spherical glass particles with diameters ranging from 36 µm to 99.8 µm

3.5 Chemo-Rheology

Chemo-rheology is used to describe the rheological behavior of cross-linking polymers during chemical reactions such as curing or vulcanization. The changes in flow behavior of cross-linking polymers is captured using rheological measurement during the curing reaction and can be used for material evaluation, process design, and process simulation. The rheological measurements also provide the most direct form of monitoring cure and capturing the gel point. Thermosets or cross-linked polymers are widely used in composites together with fiber reinforcement. They are used to manufacture structural parts in aerospace and automotive applications. Knowledge about the flow behavior of the resin within the heated mold through the fiber bed until the gel point is reached is crucial for the design and production of such parts. Thermoset rubbers such as liquid silicone rubbers (LSR) are used increasingly in the medical, automotive, and consumer markets. Part and process design require knowledge of the curing and related flow.

Figure 3.23 shows the viscosity change during curing at room temperature, the so-called cold curing. This process is used for large parts that cannot be accommodated by curing ovens. As soon as the two components are mixed, the curing process begins. The formation of chemical bonds releases heat which causes an increase in temperature. This, in turn, causes a decrease in viscosity, which eases processing of the resin, allows the exhaustion of air bubbles, and improves wetting of fillers.

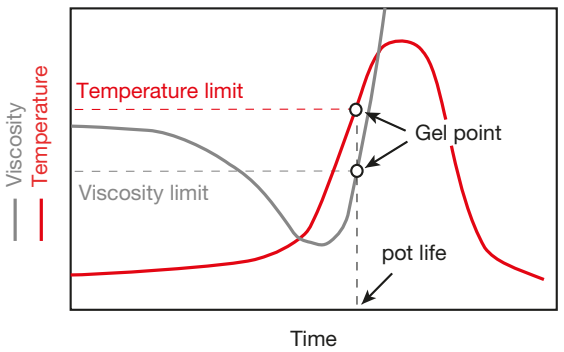

Figure 3.23 Temperature and viscosity change during cold curing [54]

As curing progresses, the viscosity increases due to the increase in molecular weight of the reacting polymers. The effect of curing eventually counteracts the decrease in viscosity caused by temperature rise, leading to a rapid rise in viscosity. As soon as the *gel point* is reached, the resin loses its ability to flow. On the time scale this point is often referred to as the pot life of the resin. The gel point is reached when the molecules are interconnected, or an infinite network is formed. After the gel point is reached, the curing reaction continues as the temperature rises until a fully cured state is reached. The chemical conversion at which the gel point is reached varies according to the molecular structure of the resin.

As an illustration of curing rates as a function of temperature, the isothermal curing history of a vinyl ester is presented in Fig. 3.24. At lower temperatures the curing starts later compared to the higher temperatures and the curing rate is slower (slope). Additionally, a lower final degree of cure is reached. The viscosity shows a comparable behavior, with a lower final viscosity value at lower temperatures, see Fig. 3.25 [55].

Rotational rheometers (see Chapter 6) have proven to be the most useful devices for investigating curing reactions of thermosetting materials, because they can capture the transitions from liquid to solid. Among these, the cone-plate and the parallel-plate systems are the most common ones, simply because they are more easily cleaned. However, some modifications are necessary to accommodate the large variations in viscosity. Just before solidification it is cumbersome to distinguish between permanent viscous deformations and recoverable contributions [56]. Therefore, it is helpful to obtain calorimetric measurements such as differential scanning calorimetry, under the same conditions.

The gel point is commonly determined by isothermal dynamic tests according to ASTM D4473 [57]. The storage (G') and loss modulus (G'') are measured at a fixed low frequency and fixed strain over a period of time. The crossover of G' and G'' is defined as the gel point as the elastic response starts to govern the viscous behavior. This point is equivalent to the point where the loss tangent reaches unity, $\tan\delta = G'/G'' = 1$.

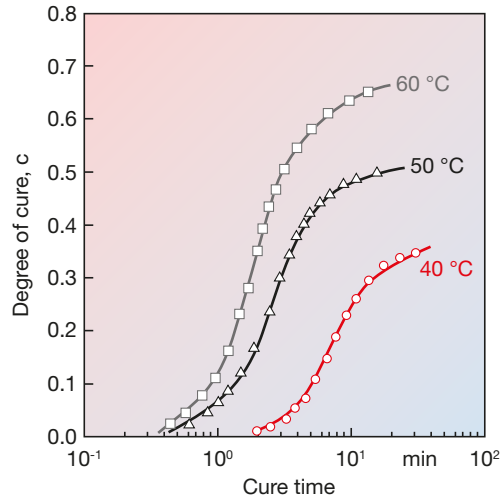

Figure 3.24 Degree of cure as a function of time for a vinyl ester at various isothermal cure temperatures

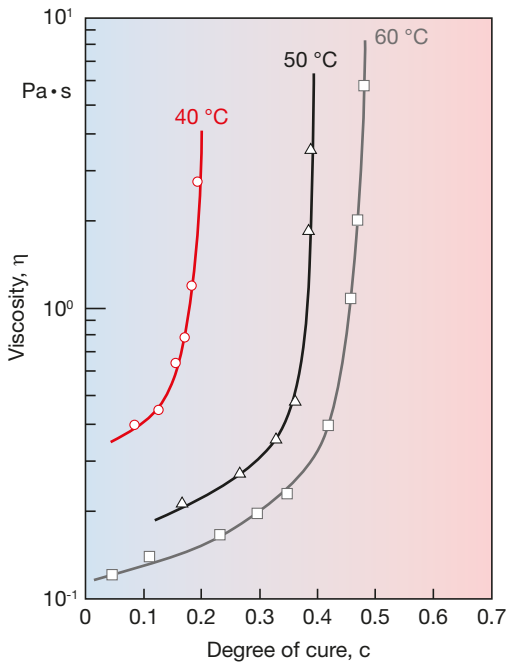

Figure 3.25 Viscosity as a function of degree of cure for a vinyl ester at various isothermal cure temperatures

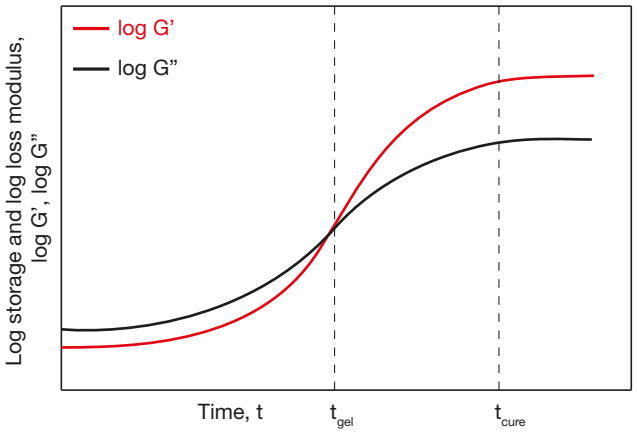

Figure 3.26 Determination of gel point by isothermal dynamic tests during cure [58]

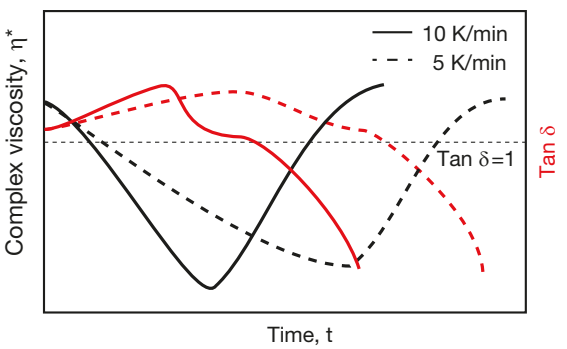

Figure 3.27 Complex viscosity and loss tangent as a function of time for different heating rates [57]

The time to reach the gel point is called the gel time, and the time at which the storage modulus levels out to a constant value is called the cure time, see Fig. 3.26. The influence of heating rate on the loss tangent and therefore the gel point as well as the complex viscosity can be seen in Fig. 3.27. At higher heating rates the gel point is reached faster.

For neat resins, the temperature corresponding to a complex viscosity η^* value of 100 Pa s after the initial heating, flowing, and onset of cure, has been suggested as the dynamic gel temperature [57].

In the first stage of injection or transfer molding processes, the effect of shear rate on viscosity is of interest. Therefore, it is often measured on the uncured resin. The strain rate dependence is dependent on the resin type. While EP and PF show shear thinning behavior, UP and PU exhibit Newtonian, strain rate independent flow behavior [59, 60]. Some measurements, especially those done without initiators,

are performed with capillary rheometers. However, as already mentioned, the most common rheometers for curing resins are rotational rheometers.

Investigations regarding the effects of fillers on the viscosity of thermosets are still in their infancy. The viscosity of the unfilled resin, the fiber content, fiber length and orientation, as well as the coupling agents influence the viscosity of the whole system [61].

A complete model for viscosity of a reacting polymer must contain the effects of temperature, T, pressure, p, strain rate, $\dot{\gamma}$, degree of cure, c, and filler properties, F [62]:

$$\eta = \eta\left(T, p, \dot{\gamma}, c, F\right) \tag{3.50}$$

There are no generalized models that include all these variables for thermosetting polymers. The different models focus either on one or two effects or on a specific material system [56]. The most common shear rate model for thermosets is the Power Law model, although the Cross model and the Newtonian models have also been used.

The effect of temperature and time are often included in form of models for cure kinetics. Extensive work has been done on the viscosity of polyurethanes [63, 64]. An empirical relation that models the viscosity of these mixing-activated polymers as a function of temperature and degree of cure, the Castro-Macosko-model, is written as

$$\eta = \eta_0 \cdot \exp\left(\frac{E}{RT}\right) \cdot \left(\frac{c_g}{c_g - c}\right)^{c_1 + c_2 c} \tag{3.51}$$

where E is the activation energy of the polymer, R is the ideal gas constant, T is the temperature, c_g is the conversion at the gel point, c the conversion, and c_1 and c_2 are constants that fit the experimental data. The most salient feature of the right term of the equation is that the viscosity increases rapidly as curing proceeds, and becomes unbound as the extent of cure approaches the extent of cure at gelation. The diffusion controlled regime after gelation is not incorporated. The fitting constants c_1 and c_2 are determined by experiments in which the viscosity is measured as a function of extent of cure at constant temperature and decreasing strain rate. Thereby, the first term on the right hand side of the equation represents the temperature dependence of the viscosity using an Arrhenius relation. In order to incorporate the shear thinning behavior of the curing polymer, a model such as the Cross model, Eq. 3.20, could be incorporated; this can be represented as

$$\eta = \frac{\eta_0(T)}{1 + \left[\frac{\eta_0(T)\,\dot{\gamma}}{\tau^*}\right]^{1-n}} \cdot \left(\frac{c_g}{c_g - c}\right)^{c_1 + c_2 c} \tag{3.52}$$

where τ^* is the critical shear stress at the transition from the Newtonian plateau η_0 to the Power Law regime, $\eta_0(T)$ the temperature dependent zero shear viscosity, and n the Power Law index.

Figure 3.28 shows the viscosity as a function of time and temperature for a polyurethane. At lower temperatures, the viscosity is initially higher, but increases more slowly because of the slower reaction rate. In the early stages of the reaction the viscosity is mainly affected by temperature.

Figure 3.29 shows the viscosity as a function of degree of cure. The Castro- Macosko model is a good fit for the described material system. It can be seen that the predicted viscosity approaches a finite value at the gel point.

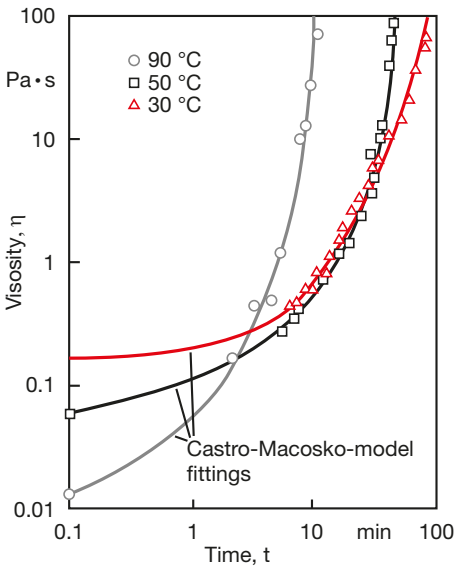

Figure 3.28
Viscosity as a function of time for a polyurethane at various isothermal cure temperatures

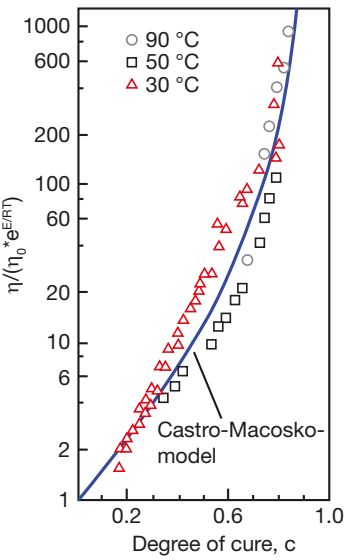

Figure 3.29
Reduced viscosity as a function of degree of cure for a polyurethane at various isothermal cure temperatures

Example 3.3 Castro-Macosko Viscosity Model

In reaction injection molding processes (RIM), polymeric parts are made directly from low viscosity (less than 10 Pa s) reactants, which cure and solidify inside the mold. For polyurethanes, the polymerization is initiated by mixing the two highly reactive components, isocyanate and polyol, inside the mold. Because the monomers are highly reactive during RIM, the mold cavity walls are maintained at low temperatures. To simulate mold filling, the rheological properties have to be known. Experiments provided the following constants [64]:

- η_0: $10.3 \cdot 10^{-8}$ Pa s
- E: 41.3 J/mol
- R (ideal gas constant): 8.3144621 J/mol K
- c_g: 0.65
- c_1: 1.5
- c_2: 1.0

In order to obtain the viscosity at 50 °C as a function of the degree of cure, the following calculation (Eq. 3.51) has to be performed for different conversion rates c, ranging from 0 to c_g = 0.65, which is shown here for a conversion of 0.1

$$\eta = 10.3 \cdot 10^{-8}\ \text{Pa s} \cdot \exp\left(\frac{41.3\ \text{J/mol}}{8.314\ \text{J/mol K} \cdot 323\ \text{K}}\right) \cdot \left(\frac{0.65}{0.65 - 0.1}\right)^{1.5+1.0\cdot 0.1}$$

$$= 2.97 \cdot 10^{-8}\ \text{Pa s}$$

Calculating for all degrees of cure provides the result shown left in Figure 3.30:

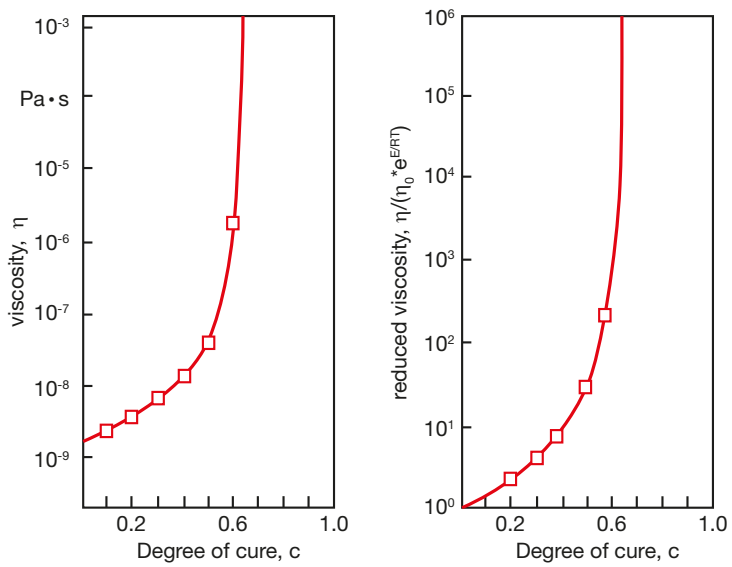

Figure 3.30 Calculated viscosity (right) and reduced viscosity (left) as functions of degree of cure for a polyurethane

Above the gel point, which here occurs at 65% cure, the right term in Eq. 3.51 cannot be solved because the base becomes negative and the exponent is not a natural number. Often, the reduced viscosity is given as a function of the degree of cure, right in Fig. 3.30, which is calculated using

$$\frac{\eta}{\eta_0 \cdot \exp\left(\frac{E}{RT}\right)} = \left(\frac{c_g}{c_g - c}\right)^{c_1 + c_2 c} \tag{3.53}$$

Example 3.4 Castro-Macosko Viscosity Model (Shear rate dependent)

For the production of flip chip packages, the so called moldable underfill (MUF) technique is used to electrically connect the die to the package carrier. The package carrier then provides the connection from the die to the exterior of the package. MUF are normally 1-component epoxies, which have to flow through a very narrow gap of 0.1 mm. In the transfer molding process, flow and heat transfer are dynamically coupled with the curing reaction. The kinetics of the curing reaction not only affect the degree of conversion of the molding compound, but also control the stresses on the overmolded structures during flow, as the viscosity increases due to the progression in degree of cure. Viscosity is influenced primarily by temperature and shear rate. Therefore, the rheological behavior of the used resins is of fundamental importance for the molding process. In order to obtain viscosity values at specific shear rates, temperatures, and conversion, the following data are needed to solve Eq. 3.52 [65]:

- n: $9.683 \cdot 10^{-3}$
- τ^*: 200 Pa
- B: $6.263 \cdot 10^{-44}$ Pa s
- T_b: $4.937 \cdot 10^{4}$ K
- c_g: 0.25
- c_1: 1.818
- c_2: −5.521

The temperature dependence of the viscosity is commonly calculated by

$$\eta_0(T) = B \cdot \exp\left(\frac{T_b}{T}\right) \tag{3.54}$$

$$\eta_0(T) = 6.263 \cdot 10^{-44}\ \text{Pa s} \cdot \exp\left(\frac{49370\ \text{K}}{423\ \text{K}}\right) = 3.05 \cdot 10^{7}\ \text{Pa s}$$

where B and T_b are constants. For example, the zero shear viscosity at 160 °C and a conversion of 0.1 and at a shear rate of 100 s^{-1} can be calculated as

$$\eta = \frac{3.05 \cdot 10^7 \text{ Pa s}}{1 + \left(\frac{3.05 \cdot 10^7 \text{ Pa s} \cdot 100 \text{ s}^{-1}}{200 \text{ Pa}} \right)^{1-n}} \cdot \left(\frac{0.25}{0.25 - 0.1} \right)^{1.818 - 5.521 \cdot 0.1} = 18.945 \text{ Pa s}$$

Calculating the viscosity for conversions of 0.05, 0.1, and 0.2 and for temperatures of 100, 150 and 200 °C as a function of shear rate gives the following results, Fig. 3.31:

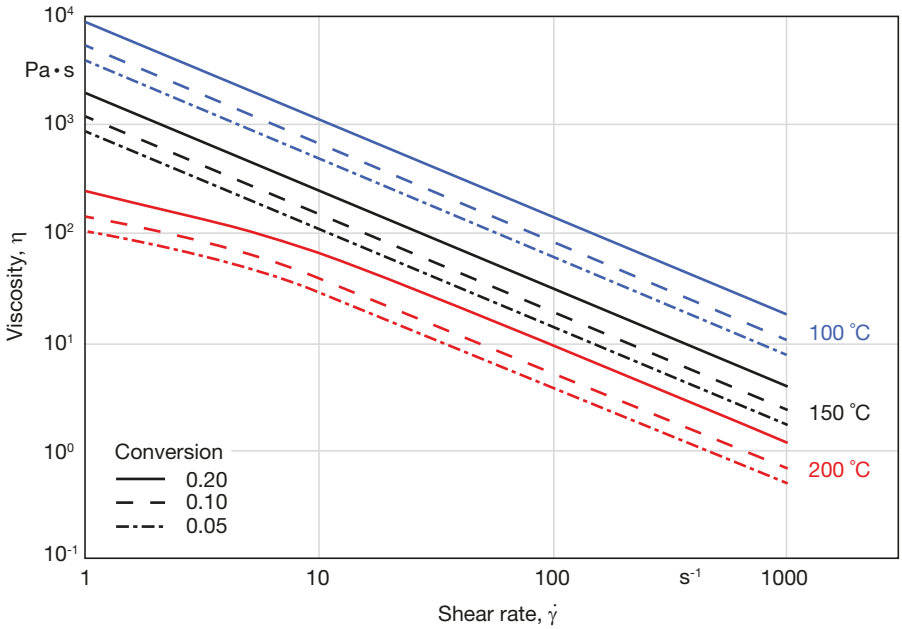

Figure 3.31 Calculated viscosity at different temperatures and degrees of cure as a function of shear rate for an epoxy (MUF)

Problems

3.1 Use the Power Law model and an exponential viscosity dependence to best fit the viscosity measurement data presented in Example 2.2.

3.2 Use the Bird-Carreau model and an Arrhenius temperature dependence to best fit the viscosity measurement data presented in Example 2.2.

3.3 Use the Cross-WLF model to best fit the viscosity measurement data presented in Example 2.2.

3.4 Use the Power Law model with a pressure shift factor b = 0.003 (see Table 3.8) to calculate the pressure dependent viscosity of PC for all given temperatures and shear rates at pressures of 100, 200, 500 and 1000 bar. What can be concluded for low shear rates?

3.5 Use the Carreau-WLF model and the parameters for PS in Table 3.5 to plot the viscosity at temperatures of 180, 200 and 220 °C and shear rates from 1 to 1,000 s^{-1}. Extend the temperature dependence with the pressure dependence using P_1 = 0.02 K/bar and a glass transition temperature T_g = 80 °C. Calculate the viscosity for pressures of 200, 400, 800 and 1200 bar.

3.6 Use Eq. 3.46 and the shear rate dependent viscosity shown in Fig. 3.18 to calculate constants a_1 and a_2. Then, using Eq. 3.48, calculate κ from the right hand side of Fig. 3.18 at a stress of 1 N/mm^2 and plot it as a function of filler volume fraction. Finally, calculate the viscosity as a function of shear rate for various volume fractions of filler and compare the calculated values with the measured values on the left hand side of Fig. 3.18. Which model works best for the shear rate dependence?

3.7 Use the parameters given in Example 3.3 to calculate the viscosity as well as the reduced viscosity as a function of degree of cure for temperatures of 30 and 90 °C and plot them in two separate diagrams. In case of multiple reactions taking place at once, the conversion will occur at a faster rate. For such a case a second order polynomial is necessary to represent the higher degree of conversion. Rewrite the right term of Eq. 3.51 to incorporate the faster degree of conversion. Using the additional constant c_3 = 2, recalculate the viscosity for temperatures of 30, 50 and 90 °C. How does the second order polynomial affect the resulting graphs compared to the previously used linear form?

3.8 Use a first order reaction model given by

$$\frac{\mathrm{d}c}{\mathrm{d}t} = a\,\mathrm{e}^{-\frac{E}{RT}}\left(1-c\right)$$

to approximate the reaction presented in Fig. 3.24. How would you improve the model?

3.9 Using the Castro-Macosko viscosity model and a first order reaction given by

$$\frac{\mathrm{d}c}{\mathrm{d}t} = a\,\mathrm{e}^{-\frac{E}{RT}}\left(1-c\right)$$

fit the viscosity data presented in Fig. 3.25.

References

[1] Arrhenius, S., The viscosity of pure liquids, Meddelanden Från K. Vetenskaps-akademiens Nobelinstitut, 3, 1–40, (1916).

[2] Laun, H. M., *Rheol. Acta, 17*, 1, (1978).

[3] Williams, M. L., Landel, R. F., Ferry, J. D., The temperature dependence of relaxation mechanisms in amorphous polymers and other glass-forming liquids, *J. Am. Chem. Soc., 77*, 3701–3707, (1955).

[4] Ferry, J. D., Viscoelastic properties of polymers, 3rd ed., Wiley, NY (1980).

[5] Van Krevelen, D. W., Properties of Polymers, 2nd ed., Elsevier, Amsterdam (1976).

[6] Tadmor, Z., Costas, G. G., Principles of polymer processing, John Wiley & Sons, Inc, Hoboken (2006).

[7] Ostwald, W., *Kolloid-Z.*, 36, 99, (1925).

[8] de Waele, A., *Oil and Color Chem. Assoc. Journal, 6*, 33, (1923).

[9] Carreau, P. J., Ph.D. Thesis, University of Wisconsin-Madison, USA, (1968).

[10] Yasuda, K., Armstrong, R. C., Cohen, R. E., *Rheol. Acta, 20*, 163, (1981).

[11] Menges, G., Wortberg, F., Michaeli, W., *Kunststoffe, 68*, 71, (1978).

[12] Cross, M. M., Rheology of non-newtonian fluids: a new flow equation for pseudo-plastic systems, *Journal of Colloid Science, 20*, 417–437, (1965).

[13] Isayev, A. I., Injection molding and compression molding fundamentals, Marcel Decker, New York (1987).

[14] Hieber, C. A., Chiang, H. H., Shear-rate-dependence modeling of polymer melt viscosity, *Polymer Engineering & Science, 32*, 931, (1992).

[15] Fetecau, C., Dobrea, D. V., Postolche, I., Overmolding injection molding simulation of tensile test specimen, *International Journal of Modern Manufacturing Technologies, 2*, p. 45–51, (2010).

[16] Garcia, J. L., Koelling, K. W., Summers, J. W., Computational prediction of PVC degradation during injection molding in rectangular channel, *Polymer Engineering & Science, 44*, 1295–1312, (2004).

[17] Barus, C., Isothermals, isopiestics and isometrics relative to viscosity. *Am. J. Sci., 45*, 87–96 (1883).

[18] Cogswell, F. N., Polymer Melt Rheology, John Wiley & Sons, New York (1981).

[19] Menges, G., Thienel, P., Wübken, G., *Kunststoffe, 60*, 42–48, (1976).

[20] Hellwege, K. H., Knappe, W., Lehmann, P., *Kolloid-Z. u. Z. Polymere, 183*, 110–119, (1962).

[21] Sedlacek, T., Zatloukal, M., Filip, P., Boldizar, A., Saha, P., *Polym. Eng. Sci., 44*, 1328, (2004).

[22] Son, Y., *J. Polym. Res., 16*, 667–671, (2009).

[23] Couch, M. A., Binding, D. M., *Polymer, 41*, 6323, (2000).

[24] Kadijk, S. E., van den Brule, B. H. A. A., On the pressure dependence of the viscosity of molten polymers, *Polym. Eng. & Sci., 34*, p. 1535–1547, (1994).

[25] Sedlacek, T., Zatloukal, M. , Lengalova, A. , Filip, P. , Saha, P., SPE ANTEC, 3748–3752, Nashville, Tennessee (2003).

[26] Amano, O., Pressure Dependent Viscosity of Polymer Melts, Proceedings of ANTEC 2000, Orlando, FL (2000).

[27] Mahishi, M., Proceedings of ANTEC 1986, Boston, MA, 547–551, (1986).

[28] Ferry, J. D., Viscoelastic properties of Polymers, Wiley, New York (1961).

[29] Bischoff, J., Catsiff, E., Tobolsky, A. V., *J. Am. Chem. Soc., 74*, 3378, (1952).

[30] Bischoff, J., Catsiff, E., Tobolsky, A. V., *J. App. Phys., 25*, 1092, (1954).

[31] Ito, K., *J. Appl. Phys., 32*, 1743, (1961).

[32] Schott, H., Kaghan, W. S., *J. Appl. Polymer Sci., 5*, 175, (1961).

[33] Vinogradov, G. V., Malkin, A. Y., *J. Polymer Sci., Part A, 2*, 2357–2372, (1964).

[34] Vinogradov, G. H., Malkin, A. Y., *J. Polymer Sci., Part A-2, 4*, 135–154, (1966).

[35] Menges, G., Wortberg, J., Michaeli, W., *Kunststoffe, 68*, 47–50, (1978).

[36] ASTM, 8.01, Plastics (I), ASTM, Philadelphia, (1994).

[37] Schümmer, P., Worthoff, R. H., *Chem. Eng. Sci., 38*, 759, (1978).

[38] Trouton, F. T., *Proc. Roy. Soc., A77*, (1906).

[39] Münstedt, H., *Rheologica Acta, 14,* 1077, (1975).

[40] Powell, P. C., Housz, A. J. I., Engineering with Polymers, CRC Press (1998).

[41] Gleißle, W., Hochgefüllte Kunststoffe, special publ. Springer-VDI Verlag, Düsseldorf, 108, (2002).

[42] Laun, H. M., Rheological properties of aqueous polymer dispersions, *Die Angewandte Makromolekulare Chemie, 123*, 335, (1984).

[43] Freundlich, H., The colloidal state: I Thixotropy, Hermann, Paris (1935).

[44] Starov, V., Zhdanov, V., Meireles, M., Molle, C., Viscosity of concentrated suspensions: influence of cluster formation, *Advances in Colloid and Interface Science, 96*, 279, (2002).

[45] Stokes, J. R., Telford, J. H., Measuring the yield behavior of structured fluids, In: *J. Non-Newtonian Fluid Mech., 124*, 137, (2004).

[46] Drummer, D., Ph.D. Thesis, LKT, University of Erlangen-Nuremberg, Germany (2004).

[47] Einstein, A., *Ann. Physik, 19*, 549, (1906).

[48] Guth, E., Simha, R., *Kolloid-Zeitschrift, 74*, 266, (1936).

[49] Guth, E., *Proceedings of the American Physical Society*, (1937); *Physical Review, 53*, 321, (1938).

[50] Batchelor, G. K., *Annu. Rev. Fluid Mech., 6*, 227, (1974).

[51] Geisbüsch, P., Ph.D. Thesis, IKV, RWTH-Aachen, Germany, (1980).

[52] Gupta, R. K., Flow and Rheology in Polymer Composites Manufacturing, Ed. S. G. Advani, Elsevier, Amsterdam, (1994).

[53] Milliken, W. J., Powell, R. L., Flow and Rheology in Polymer Composites Manufacturing, Ed. S. G. Advani, Elsevier, Amsterdam, (1994).

[54] Ehrenstein, G. W., Polymeric Materials, Hanser Publisher, Cincinatti (2004).

[55] Han, C. D., Lem, K. W., *J. Appl. Polym. Sci., 29*, 1879, (1984).

[56] Halley, P. J., Mackay, M. E., Chemorheology of Thermosets – An Overview, *Polym. Eng. Sci., 36*, 593, (1996).

[57] ASTM D4473, Plastics (I), Dynamic Mechanical Properties: Cure Behavior, ASTM, Philadelphia, (2008).

[58] Mezger, T., Das Rheologie Handbuch, Vincentz, Hannover (2000).

[59] Sundstrom, D. W., Burkett, S. J., *Polym. Eng. Sci., 21*, 1108, (1981).

[60] Hartley, M. D., Williams, H. L., *Polym. Eng. Sci., 21*, 135, (1981).

[61] Han, C. D., Multiphase Flow in Polymer Processing, Academic Press, New York (1981).

[62] Ryan, M. E., *Polym. Eng. Sci., 24*, 358, (1984).

[63] Castro, J. M., Macosko, C. W., *AIChe J., 28*, 250, (1982).

[64] Castro, J. M., Perry, S. J., Macosko, C. W., *Polymer Comm., 25*, 82, (1984).

[65] Tamil, J., Ore, S. H., Gan, K. Y., Bo, Y. Y., Ng, G., Wah, P. T., Suthiwongsunthorn, N., Chungpaiboonpatana, S., *Journal Micro. and Elect. Pack., 9*, 19, (2012).